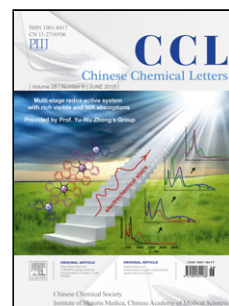# Accepted Manuscript

Communication

D-A structured high efficiency solid luminogens with tunable emissions: molecular design and photophysical properties

Yunzhong Wang[a,†], Zihan He[a, †], Gan Chen[a], Tong Shan[b], Wangzhang Yuan[a,*] , Ping Lu[b, *], Yongming Zhang[a, *]

[a]*School of Chemistry and Chemical Engineering, Shanghai Key Lab of Electrical Insulation and Thermal Aging, Shanghai Electrochemical Energy Devices Research Center, Shanghai Jiao Tong University, Shanghai 200240, China*

[b]*State Key Laboratory of Supramolecular Structure and Materials, Jilin University, Changchun 130012, China*

∗ Corresponding authors.

E-mail address: wzhyuan@sjtu.edu.cn (W.Z.Y.), lup@jlu.edu.cn (P.L.), ymzsjtu@gmail.com (Y.Z.).

† These authors contribute equally to this work

graphical abstract
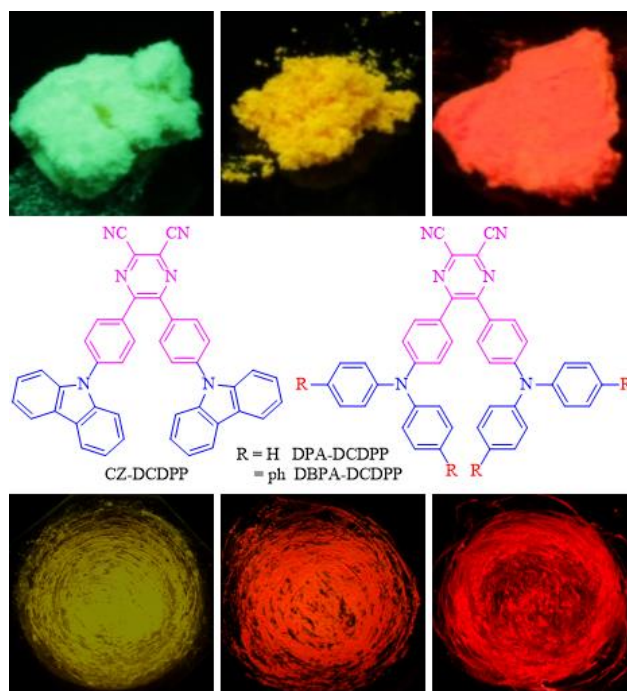
The combination of an electron-accepting unit with aggregation-induced emission features and varying electron-donating arylamines yields high efficiency solid luminogens with tunable emissions from green to red.

ARTICLE INFO   ABSTRACT

Please donot adjust the margins

Fabrication of efficient solid luminogens with tunable emission is both fundamentally significant and technically important. Herein, based on our previous strategy for the construction of efficient and multifunctional solid luminogens through the combination of diverse aggregation-induced emission (AIE) units with other functional moieties, a group of luminophores with electron donor-acceptor (D-A) structure and typical intramolecular charge transfer (ICT) characteristics, namely CZ-DCDPP, DPA-DCDPP and DBPA-DCDPP were synthesized and investigated. The presence of twisting and AIE-active 2,3-dicyano-5,6-diphenylpyrazine (DCDPP) moiety endows them highly emissive in the solid states, whereas the introduction of arylamines with varied electron-donating capacity and different conjugation render them with tunable solid emissions from green to red. While CZ-DCDPP and DPA-DCDPP solids exhibit distinct mechanochromism, both DPA-DCDPP and DBPA-DCDPP solids can generate efficient red emission. Owing to their high efficiency, remarkable thermal and morphological stabilities and moreover red emission, they are promising for diverse optoelectronic and biological applications.

High efficiency solid emitters have attracted intense attention owing to their promising applications in organic light-emitting diodes (OLEDs) [1–4], organic lasers [5], chemo- and bio-sensing [6–8], bioimaging [9–11], and so on. Conventional luminogens with remarkable conjugation are generally highly emissive in solutions, while being weakly luminescent or even totally quenched when aggregated, demonstrating aggregation-caused quenching (ACQ) effect [12]. Contrary to the ACQ luminogens, in 2001, Tang's group reported the aggregation-induced emission (AIE) phenomenon of a propeller like silole [13], which is practically nonluminescent in solutions, but become intensely emissive upon aggregation. The discovery of AIE phenomenon opens a new avenue to the fabrication of efficient solid emitters [14–21].

Furthermore, the transformation of ACQ chromophores into AIE luminogens (AIEgen) is developed by simple decoration of ACQ dyes with AIE units in 2010 [22], thus paving the way for the construction of diverse high efficiency solid luminogens. Notably, it also affords a facile approach to the construction of multifunctional luminogens through incorporation of other functional moieties like electron-donating (D) [22–23] or electron-accepting (A) groups (Fig. 1a) [24]. Later, through introduction of typical D and A units, efficient solid luminophores with both AIE and intramolecular charge transfer (ICT) characteristics were obtained [25]. Further functionalization of triphenylamine (TPA) with a typical AIE structure, namely triphenylethene (HTPE) [26], results in solution-solid dual state efficient luminogens owing to the conjugation-induced rigidity (CIR) effect in twisted molecules (Fig. 1a) [27]. Derived from these previous results, it is envisioned that efficient solid luminogens with tunable emission colors can be constructed through combination of D and A building blocks accompanying the incorporation of AIE moieties. Modulation of the strength of the D and A groups can readily tune the emission color [25,28,29], whereas AIE units may offer the resulting compounds with efficient solid emission [22,24].

To check the feasibility of above conjecture, herein, we synthesized a group of luminogens consisting of 2,3-dicyano-5,6-diphenylpyrazine (DCDPP) [30] and arylamines of carbazole (CZ), diphenylamine (DPA)and di[(1,1'-biphenyl)-4-yl]amine (DBPA). DCDPP was chosen because of its twisting structure, AIE feature and strong electron-accepting capacity [30], while CZ, DPA and DBPA were adopted on account of their varying electron-donating strengths and different conjugation lengths. The target compounds were successfully synthesized through a two-step procedure (Scheme S1 in Supporting information). Briefly, the important benzil derivatives were obtained by the palladium catalyzed C–N coupling reaction between 4,4′-dibromobenzil and corresponding arylamines. Subsequent cyclization reactions between them and 2,3-diaminomaleonitrile readily produced resulting compounds in moderate to high yields (63%~88%). The compounds were spectroscopically characterized, with satisfactory results obtained (Figs. S1–S3 in Supporting information).Indeed, CZ-DCDPP, DPA-DCDPP [46] and DBPA-DCDPP (Fig. 1b) were characterized with efficient solid emission and well tunable photophysical properties. Furthermore, DPA-DCDPP and DBPA-DCDPP can demonstrate red emission with high efficiency up to 43.0%, which render them highly possible for optoelectronic and biological applications [9,31–34].

Absorption spectra of CZ-DCDPP, DPA-DCDPP and DBPA-DCDPP in different solvents are slightly varied, with peaks and shoulders at 292/324/334/409, 298/412/459 and 324/429/469 nm in toluene (Fig. S4 in Supporting information), respectively. While the peaks at the shorter wavelength region (292, 298, 324 nm) can be attributed to the π-π* transitions, those at longer wavelength region (409, 412/459, 429/469 nm) are assignable to the ICT transitions. These absorption peaks, on one hand, indicate the gradually enhanced effective conjugation length; on the other hand, suggest enhanced electron donating ability of the arylamines. Both factors would impact on the emission properties of the luminogens.

Their emission spectra, however, are red-shifted with increasing solvent polarity, accompanying with decreased intensity (Fig. 2), which is typically observed in ICT luminogens [25,28]. Taking DPA-DCDPP for an example, the emission peak shifts from 547 nm in toluene to 608 nm in tetrahydrofuran (THF) and 623 nm in dichloromethane (DCM) [35]. Meanwhile, CZ-DCDPP, DPA-DCDPP and DBPA-DCDPP emit bright green, greenish-yellow and yellowish-orange lights in low-polarity toluene, with emission peaks at 515, 547 and 565 nm (Fig. 2), respectively. Similar red-shifted emission is also observed for the luminogens in THF and DCM (Fig. 2, Table S1 in Supporting information). Such trend in both low- and high-polarity solvents indicates that the effective conjugation length and the ICT effect gradually increase in the order of CZ-DCDPP, DPA-DCDPP and DBPA-DCDPP. Owing to the highest ICT strength, DBPA-DCDPP is most sensitive to the solvent polarity, and almost no emission is observed in THF (Fig. 2). These results verify the effective modulation of the emission of the luminogens by tuning their effective conjugation length and ICT strength.

Their emission in THF and THF/water mixtures were further monitored to gain more insights into the ICT and aggregation effects. As exampled in Fig. S5 in Supporting information, when dissolved in THF, DPA-DCDPP depicts red emission with moderate intensity. Adding a small fraction of water (f_w) of 10% into THF strikingly weakens its emission, making it almost nonemissive owing to the increased solvent polarity. Increasing of f_w does not change the intensity much until it reaches 70%, at which the intensity starts to increase due to the predominant aggregation effect, which is helpful to the conformation rigidification and light emission. Further addition of water affords more intensified emission at around 606 nm. DBPA-DCDPP exhibits similar emission behaviors to those of DPA-DCDPP with more prominent AIE effect (Fig. S6 in Supporting information). However, CZ-DCDPP achieves its maximal intensity at f_w = 60%, further addition of water reduces its emission (Fig. S7 in Supporting information). At f_w = 95%, the emission intensity is even lower than that in THF, which should be ascribed to the presence of detrimental exciton interactions in the nanoaggregates.

Owing to the incorporation of AIE-active DCDPP moiety, the twisting structure and ICT nature, these luminogens are expected to be highly emissive in the solid state [22–25,27]. Indeed, the recrystallized solid powders of CZ-DCDPP, DPA-DCDPP and DBPA-DCDPP demonstrate intense green, yellow and red emission upon irradiation, with emission maxima/efficiencies of 527 nm/12.8%, 577 nm/20.0% and 624 nm/43.0% (Fig. 3), respectively, indicative of their efficient and tunable emissions. Notably, among these luminogens, the efficiency of CZ-DCDPP is the lowest, while that of DBPA-DCDPP is the highest, which appears to be counterintuitive because luminogens normally tend to be less emissive with enhanced ICT effect. Despite the detailed reasons remains unclear yet, it is speculated that various molecular structures might be accountable for it. While CZ is planar, DPA and DBPA units are twisted, thus relatively less or blocked quenching by exciton interactions can be expected in the latter two luminogens because of steric hindrance. Meanwhile, compared to DPA-DCDPP, conformation rigidity of DBPA-DCDPP in the neat solid might be enhanced due to better conjugation and much greater steric hindrance, thus making it emits more efficiently even in the redder region.

The twisting structure and efficient solid emission of the luminogens make them highly promising as mechanochromic candidates [14,36–41], which can be used in security ink, data recording and anti-counterfeiting. Upon manual grinding, CZ-DCDPP and DPA-DCDPP exhibit distinct emission color change from green/yellow to yellow/red (565/615 nm) with broadened full width at half maxima (FWHM) (Fig. 3d), thus testifying their mechanochromism. DBPA-DCDPP, however, displays relatively slight variations in color and emission peak. Such mechanochromism should be ascribed to the conformation planarization and potentially excimer formation upon grinding, which is associated with the conversion from crystalline (twisted) to amorphous (planarized) states (Fig. 3e). The small change of DBPA-DCDPP might be attributed to its larger steric hindrance and lower degree of conformation planarization, as well as much lower crystallinity after recrystallization (Fig. 3e). Notably, the mechanochromism is also reversible. Upon fuming with DCM vapor, the ground solids of DPA-DCDPP restore to its original green emission accompanying the recovery of emission spectrum and crystalline XRD pattern (Fig. 3).

Thermal and morphological stabilities of the luminogens are crucial to the performance and lifetime in their optoelectronic applications [42,43]. Thermal decomposition temperature (T_d, at which a sample loses its 5% weigh) and glass transition temperature (T_g) of the luminogens were thus measured. As derived from the thermogravimetric analysis (TGA) and differential scanning calorimeter (DSC) results, the T_d/$T_g$values forCZ-DCDPP, DPA-DCDPP and DBPA-DCDPP are 430/- [44], 372/104 and 427/151 °C (Figs. S8 and S9in Supporting information), respectively, suggestive of their good thermal and morphological stabilities.

Owing to the high solid efficiency, excellent thermal and morphological stabilities, as well as red light emission at amorphous state, DPA-DCDPP and DBPA-DCDPP are promising for OLED applications. Their electroluminescence (EL) performances were thus studied. We first tried the nondoped devices with the general configuration of ITO/HATCN/NPB/TCTA/X/TPBi/LiF/Al [45], where ITO and LiF/Al are the anode and bilayer cathode, respectively, HATCN serves as an anode buffer layer to enhance the hole injection, NPB and TPBi are the hole transport layer (HTL) and electron transport layer (ETL), respectively, TCTA acts as the electron-blocking layer (EBL), and X represents the light emitting layer (LEL). The performances of devices I (X = DPA-DCDPP) and II(X = DBPA-DCDPP) are shown in Fig. 4 and summarized in Table 1. Both devices turn on at a low voltage of 2.9 V, giving red EL at620 and 632 nm, respectively, which are close to those of ground powders of DPA-DCDPP (615 nm) and DBPA-DCDPP(634 nm), suggestive of their amorphous nature in the devices. The Commission Internationale de L'Eclairage (CIE) coordinates, maximalluminance(L_{max}),current efficiency (LE_{max}), power efficiency (PE_{max}) and external quantum efficiency (EQE_{max}) for devices I/II are (0.61, 0.38)/(0.64, 0.35),

10080/12370 cd/m^2, 1.31/1.70 cd/A, 1.25/1.67 lm/W and 1.07%/1.78%, respectively. It is rare to obtain the red EL with such relatively good performances, especially for the nondoped devices.

[a] Device configuration: ITO/HATCN (6 nm)/x/LiF (1.2 nm)/Al (120 nm), x= NPB (40 nm)/TCTA (5 nm)/DPA-DCDPP (30 nm)/TPBi (35 nm) (I), NPB (30 nm)/TCTA (5 nm)/DBPA-DCDPP (30 nm)/TPBi (45 nm) (II), NPB (40 nm)/TCTA (5 nm)/CBP:DPA-DCDPP 15 wt% (30 nm)/TPBi (35 nm) (III), NPB (25 nm)/TCTA (10 nm)/CBP:DBPA-DCDPP 15 wt% (30 nm)/TPBi (45 nm) (IV). [b] At the luminance of 1 cd/m^2. [c] At the driving voltages of 4 (I, III) and 5 V (II, IV).

Since doping can normally improve the OLED performance [46], we thus constructed devices with 15 wt% DPA-DCDPP (III) and DBPA-DCDPP (IV) doped into the CBP [45] host as LELs. As can be seen from Fig. 4 and Table 1, the devices demonstrate blue-shifted yellow and orange emissions at 580 and 596 nm owing to the relatively low polarity of CBP. The EL luminance and efficiencies, however, are remarkably boosted, with L_{max}, LE_{max}, PE_{max} and EQE_{max} of 16 280/22 790 cd/m^2, 3.83/6.26 cd/A, 3.76/5.96 lm/W and 1.50%/3.04% for devices III and IV, respectively. Such greatly enhanced efficiencies might be ascribed to the smoother contact and balance charge transport in the doped devices compared to their nondoped counterparts. Meanwhile, the relatively better performances of both nondoped and doped devices of DBPA-DCDPP compared to those of DPA-DCDPP might be ascribed to its much higher emission efficiency. These results highly suggest the fabrication of OLEDs with tunable EL color and efficiencies by using these luminogens. It is also believed that the performances of the devices can be further promoted upon optimization.

In summary, facile combination of AIE-active electron-accepting moiety with varying electron-donatingarylamines generates D-A structured high efficiency solid luminogens, $i.e.$, CZ-DCDPP, DPA-DCDPP and DBPA-DCDPP, with tunable photophysical properties. While the crystalline solids of CZ-DCDPP and DPA-DCDPP exhibit distinct mechanochromism from green and yellow to yellow and red emissions upon grinding, DBPA-DCDPP demonstrate efficient red emission at both crystalline and amorphous states with high efficiency up to 43%. Owing to their excellent thermal and morphological stabilities, both doped and nondoped OLED devices with good performances were fabricated based on DPA-DCDPP and DBPA-DCDPP. Notably, the nondoped devices demonstrate red EL with high luminance and EQE_{max} of 1.78%. Furthermore, considering theexcellent red solid emission of DPA-DCDPP (amorphous) and DBPA-DCDPP (crystalline and amorphous), they are highly applicable in biological and biomedical areas.

Acknowledgment

References

[1] L. Yao, S. Zhang, R. Wang, et al., Angew. Chem. Int. Ed. 53 (2014) 2119–2123.

[2] S. Wang, X. Yan, Z. Cheng, et al., Angew. Chem. Int. Ed. 54 (2015) 13068–13072.

[3] W.C. Chen, Y. Yuan, S.F. Ni, et al., Chem. Sci. 8 (2017) 3599–3608.

[4] Y.J. Luo, Z.Y. Lu, Y. Huang, Chin. Chem. Lett. 27 (2016) 1223–1230.

[5]M. Fang, J. Huang, Y. Zhang, et al., Mater. Chem. Front. 1 (2017) 668–676.

[6]D. Ding, K. Li, B. Liu, B.Z. Tang, Acc. Chem. Res. 46 (2013) 2441–2453.

[7] M. Wang, G. Zhang, D. Zhang, D. Zhu, B.Z. Tang, J. Mater. Chem. 20 (2010) 1858–1867.

[8] C. Ge, Y. Liu, X. Ye, et al., Mater. Chem. Front. 1 (2017) 530–537.

[9] H. Lu, Y. Zheng, X. Zhao, et al., Angew. Chem. Int. Ed. 55 (2016) 155–159.

[10] Q. Wan, R. Jiang, L. Mao, et al., Mater. Chem. Front. 1 (2017) 1051–1058.

[11] J. Qian, Z. Zhu, C.W.T. Leung, et al., Biomed. Opt. Express 6 (2015) 1477–1486.

[12] Y. Kubota, J. Uehara, K. Funabiki, M. Ebihara, M. Matsui, Tetrahedron Lett. 51 (2010) 6195–6198.

[13] J. Luo, Z. Xie, J.W.Y. Lam, et al., Chem. Commun. 381 (2001) 1740–1741.

[14] W.Z. Yuan, Y. Tan, Y. Gong, et al., Adv. Mater. 25 (2013) 2837–2843.

[15] J. Mei, N.L.C. Leung, et al., Chem. Rev. 115 (2015) 11718–11940.

[16] M. Chen, L. Li, H. Nie, et al., Chem. Sci. 6 (2015) 1932–1937.

[17] P.C. Shen, Z.Y. Zhuang, Z.J. Zhao, B.Z. Tang, Chin. Chem. Lett. 27 (2016) 1115–1123.

[18] S. Xu, T. Liu, Y. Mu, et al., Angew. Chem.Int. Ed. 54 (2015) 874–878.

[19] Z. Wang, B. Xu, L. Zhang, et al., Nanoscale 5 (2013) 2065–2072.

[20] Y. Dong, J.W.Y. Lam, A. Qin, et al., J. Sun, H.S. Kwok, Appl. Phys. Lett. 91 (2007) 011111.

[21] T. Han, X. Feng, B. Tong, et al., Chem. Commun. 48 (2012) 416–418.

[22] W.Z. Yuan, P. Lu, S. Chen, et al., Adv. Mater. 22 (2010) 2159–2163.

[23] Y. Liu, S. Chen, J.W.Y. Lam, et al., Chem. Mater. 23 (2011) 2536–2544.

[24] W.Z. Yuan, S. Chen, J.W.Y. Lam, et al., Chem. Commun. 47 (2011), 11216–11218.

[25] W.Z. Yuan, Y. Gong, S. Chen, et al., Chem. Mater. 24 (2012) 1518–1528.

[26] Z. Yang, Z. Chi, T. Yu, et al., J. Mater. Chem. 19 (2009) 5541–5546.

[27] G. Chen, W. Li, T. Zhou, et al., Adv. Mater. 27 (2015) 4496–4501.

[28] R. Hu, E. Lager, A. Aguilar-Aguilar, et al., J. Phys. Chem. C 113 (2009) 15845–15853.

[29] Y.W. Lu, Y.Q. Tan, Y.Y. Gong, et al., Chin. Sci. Bull. 58 (2013) 2719–2722.

[30] A. Qin, J.W.Y. Lam, F. Mahtab, et al., Appl. Phys. Lett. 94 (2009) 2007–2010.

[31] B. Gao, Q. Zhou, Y. Geng, et al., Mater. Chem. Phys. 99 (2006) 247–252.

[32] X. Zhang, M. Liu, B. Yang, et al., Polym. Chem. 4 (2013) 5060–5064.

[33] Q. Zhao, K. Li, S. Chen, et al., J. Mater. Chem. 22 (2012) 15128–15135.

[34] X. Han, Q. Bai, L. Yao, et al., Adv. Funct. Mater. 25 (2015) 7521–7529.

[35] The emission maxima of the compounds in DMF are difficult to be accurately identified even after signal amplification, owing to their rather low intensities.

[36] Z. Chi, X. Zhang, B. Xu, et al., Chem. Soc. Rev. 41 (2012) 3878–3896.

[37] W.B. Li, W.J. Luo, K.X. Li, W.Z. Yuan, Y.M. Zhang, Chin.Chem. Lett. 28 (2017) 1300–1305.

[38] Z. Ma, Z. Wang, X. Meng, et al., Angew. Chem. Int. Ed. 55 (2016) 519–522.

[39] Y. Gong, Y. Tan, J. Liu, et al., Chem. Commun. 49 (2013) 4009–4011.

[40] X.Y. Teng, X.C. Wu, Y.Q. Cao, et al.,Chin. Chem. Lett. 28 (2017) https://doi.org/10.1016/j.cclet.2017.02.018.

[41] C. Hang, H.W. Wu, L.L. Zhu, Chin. Chem. Lett. 27 (2016) 1155–1165.

[42] S.L. Tao, Z.K. Peng, X.H. Zhang, et al., Adv. Funct. Mater. 15 (2005) 1716–1721.

[43] J. Huang, N. Sun, Y. Dong, et al. Adv. Funct. Mater. 23 (2013), 2329–2337.

[44] No glass transition was observed for CZ-DCDPP during the measurement.

[45] ITO = indium tinoxide, HATCN = 1,4,5,8,9,11-hexaazatriphenylene hexacarbonitrile (HATCN), NPB = *N,N′*-bis(naphthalen-1-yl)-*N,N′*-bis(phenyl)benzidine, TCTA = tris(4-carbazoyl-9-ylphenyl)amine, TPBi = 1,3,5-tris(1-phenyl-1H-benzimidazol-2-yl)benzene, CBP = 4,4′-bis(9-carbazolyl)-2,2′-biphenyl.

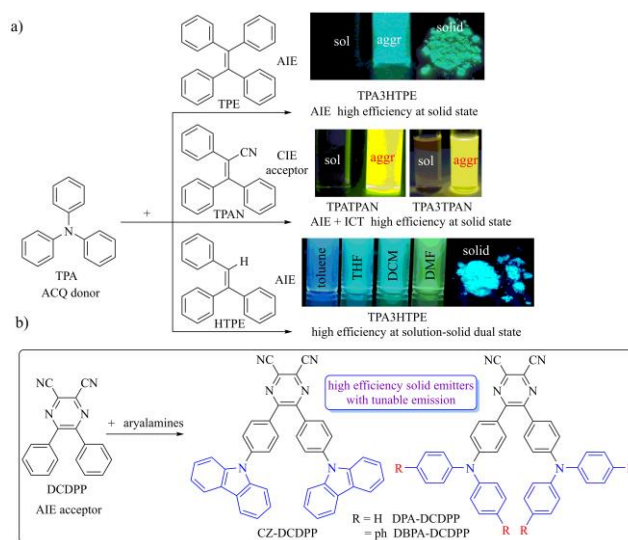[46] L. Xu, Y. Zhao, G. Long, et al., RSC Adv. 5 (2015) 63080–63086.

Fig. 1. (a) Examples for the fabrication of efficient solid emitters through the incorporation of AIE units. (b) Illustration of the design concept of this work. Photographs in (a) were reproduced from ref. [14, 22, 25, 27], with permissions from John Wiley and Sons (ref. [14, 22, 27]) and American Chemistry Society (ref. [25]), respectively.
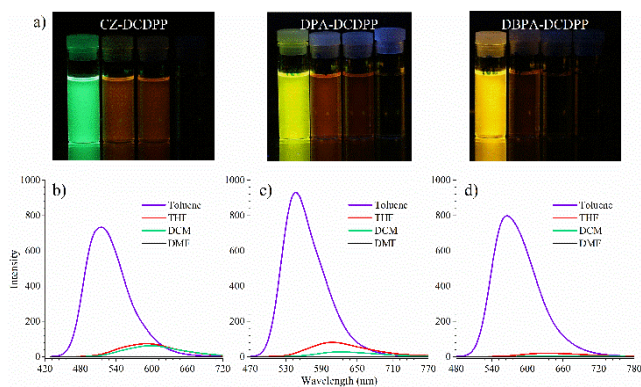

Fig. 2. (a) Photographs taken under 365 nm UV illumination and (b-d) emission spectra of corresponding solutions of (b) CZ-DCDPP, (c) DPA-DCDPP and (d) DBPA-DCDPP in different solvents (from left to right: toluene, THF, DCM and DMF). Concentration = 10 μmol/L.
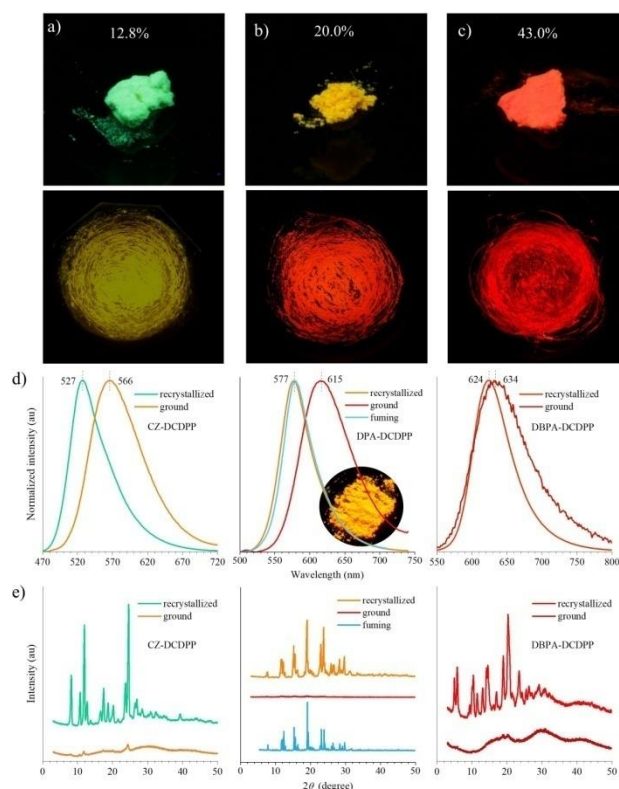
Fig. 3. (a–c) Photographs of recrystallized (upper) and ground (lower) solids of (a) CZ-DCDPP, (b) DPA-DCDPP and (c) DBPA-DCDPP under 365 nm UV illumination.(d) Emission spectra and (e) XRD patterns of different solid powders of CZ-DCDPP, DPA-DCDPP and DBPA-DCDPP. Emission efficiencies of the recrystallized powders are indicated in (a). The inset in (d) is the photograph of the fumed solid of DPA-DCDPP under 365 nm UV illumination.
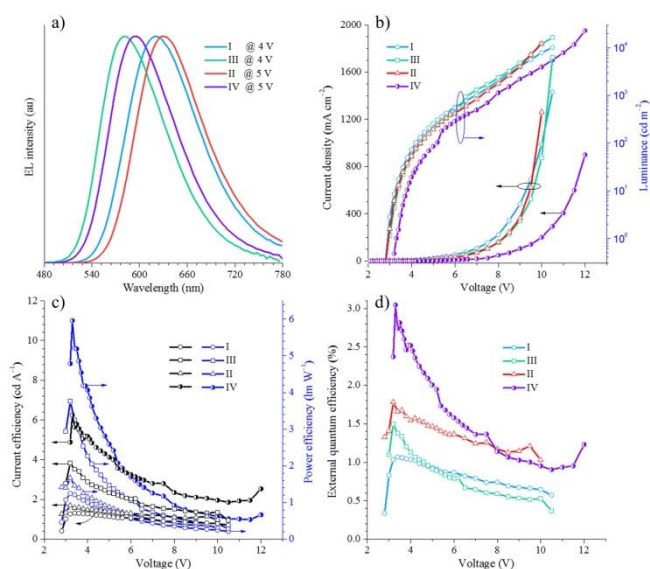

Fig. 4. (a) EL spectra of devices I-V based on DPA-DCDPP and DBPA-DCDPP. (b) Current density−voltage−luminance plots, (c) current efficiency−voltage−power efficiency plots, and (d) external quantum efficiency−voltage plots of their nondoped (I and II) and doped (III and IV) multilayer OLED devices. Device configurations are given in Table 1.

Table 1 Performance of EL devices of DPA-DCDPP and DBPA-DCDPP.

Device[a]	V_{on}[b]	L_{max}	LE_{max}	PE_{max}	EQE_{max}	λ_{max}[c]	CIE[c]

Please donot adjust the margins

	(V)	(cd/m²)	(cd/A)	(lm/W)	(%)	(nm)	(x,y)
I	2.9	10 080	1.31	1.25	1.07	620	(0.61,0.38)
II	2.9	12 370	1.70	1.67	1.78	632	(0.64,0.35)
III	2.9	16 280	3.83	3.76	1.50	580	(0.52,0.47)
IV	3.3	22 790	6.26	5.96	3.04	596	(0.56,0.43)

	(V)	(cd/m²)	(cd/A)	(lm/W)	(%)	(nm)	(x,y)